Journal of Materials Chemistry C

PAPER

View Article Online
View Journal | View Issue



Cite this: J. Mater. Chem. C, 2017, 5, 4661

# An RGH–MOF as a naked eye colorimetric fluorescent sensor for picric acid recognition†

Yihe Zhang,[ab] Bin Li, *[a] Heping Ma,*[a] Liming Zhang[a] and Wenxiang Zhang[ab]

Received 3rd March 2017,
Accepted 10th April 2017

DOI: 10.1039/c7tc00936d

rsc.li/materials-c

Lanthanide metal–organic frameworks (MOFs) are considered as promising sensing materials in picric acid (PA) detection. Designing and preparing fluorescence enhancement sensors, however, are challenges due to the electron deficient properties of PA. Multifunctional MOF materials with guest dyes introduced into host MOFs have aroused great interest for various applications recently. Herein a ratiometric fluorescent sensor (denoted as RGH–Eu(BTC)) for PA recognition was developed by immobilizing a rhodamine derivative (RGH) onto the surface of lanthanide MOFs (Eu(BTC)). In the presence of acidic PA, the fluorescence of red emission was quenched by the donor–acceptor electron transfer process and green emission was caused by the spirolactam ring-opening of rhodamine. In addition, the color of the sensor system was changed from colorless to orange, which could be distinguished easily by the naked eye. RGH–Eu(BTC) also demonstrated high selectivity toward PA among nitroaromatic compounds and organic carboxylic acids in solution. This work established a very promising strategy for the simple, accurate and instantaneous sensing of PA in practical applications.

## Introduction

Picric acid (2,4,6-trinitrophenol, PA) is recognized as a primary ingredient of explosive material, and has a higher explosive power than 2,4,6-trinitrotoluene (TNT).[1] It can also be used in dye manufacturing, antiseptics, and pharmaceuticals.[2,3] Due to its high biotoxicity, the release of PA into the environment may threaten our ecosystem and human health.[4,5] Moreover, the natural degradation of PA is very difficult because of its electron-deficient character.[6,7] Various methods such as trained canines, gas chromatography, metal detectors, surface-enhanced Raman spectroscopy (SERS), and ion mobility spectrometry (IMS) have been established to detect PA.[8–10] In addition, fluorescence-based sensors are one of the priority technologies for PA detection benefiting from their low cost, rapid response, good portability, high sensitivity and selectivity.[11,12] However, most of the fluorescent sensors for PA are based on a "turn off" response, which may be easily affected by background fluorescence or other environmental interference factors.[13–15] In general, "turn on" fluorescent sensors for analytes are more preferred than the "turn off" ones, because of the fact that the appearance of emission is more easily identified than the dimming of a bright emission by the naked eye.[4,16,17] Due to the electron-deficient character of the PA molecule, designing a sensor with fluorescent emission enhancement is still a challenge.

Metal–organic framework (MOF) materials have potential applications in many fields such as gas storage, dye separation, catalysis and drug delivery.[18,19] In the last few years, design and synthesis of luminescent MOFs which could be used as explosives sensors have aroused researchers' attention.[20] Among the luminescent MOFs classified, lanthanide MOFs have been selected as excellent candidates for nitroaromatic explosive detection. However, most applications are limited by single-emission quenching which may suffer interference by uncontrollable factors. Compared with the traditional use of MOFs for dye adsorption, host–guest systems (dye–MOF) have been recently studied to obtain dual-emitting MOFs. Many research studies have focused on exploring dye–MOFs as white emission materials or sensors for organic solvent molecules and metal ions.[19,21,22] Although these works have proved that these host–guest systems can be self-calibrated in sensing organic solvent molecules, research studies about PA recognition based on ratiometric fluorescent dye–MOF systems, especially displaying an inversely proportional relationship, are rarely reported.[23]

Herein, we report a novel PA sensor by immobilizing a rhodamine probe (RGH) onto the surface of a luminescent lanthanide MOF (Eu(BTC)), namely, RGH–Eu(BTC). The luminescent MOF can be used as both a recognition unit and an internal reference in PA detection, and the rhodamine derivative is employed as a fluorescent "turn-on" probe through structural transformation. This RGH–Eu(BTC) material possesses several

[a] State Key Laboratory of Luminescence and Applications, Changchun Institute of Optics Fine Mechanics and Physics, Chinese Academy of Sciences, Changchun 130033, P. R. China. E-mail: libinteacher@163.com, mahp@ciomp.ac.cn
[b] University of Chinese Academy of Sciences, Beijing 100039, P. R. China

† Electronic supplementary information (ESI) available: SEM images, FTIR spectra, elemental analysis data, and other experimental data. See DOI: 10.1039/c7tc00936d

advantages in PA detection: firstly, with an increase in PA, the green emission signal of RGH is increased greatly, which reduces the effect of background fluorescence and other environmental interference factors. Secondly, the color of RGH–Eu(BTC) changes from colorless to orange, which can be observed easily by the naked eye. Thirdly, the emission of rhodamine and Eu can construct a ratiometric luminescent sensor. Finally, the nanosensor exhibits high selectivity toward PA among nitroaromatics and acidic analytes.

# Experimental section

### Chemicals and materials

The initial chemicals, including $Eu_2O_3$ (99.9%), 1,3,5-benzenetricarboxylic acid ($H_3BTC$), sodium acetate trihydrate (NaAc) rhodamine 6G (RG), hydrazine hydrate ($N_2H_4{\cdot}H_2O$, 85%) 1-ethyl-3-(3-dimethylaminopropyl)carbodiimide hydrochloride (EDC), and *N*-hydroxysuccinimide (NHS), were purchased from commercial sources. $Eu(NO_3)_3{\cdot}6H_2O$ was obtained by dissolving $Eu_2O_3$ in concentrated nitric acid with agitation until the solution became clear and colorless, and then the solution was heated to dryness. Unless otherwise mentioned, all chemicals were of AR grade and used as received. Double distilled water was used in this work.

**Caution!** PA, TNT and other nitroaromatic compounds have highly explosive characters. They should be used with the best safety precautions and extreme care. Only small quantities can be handled in the testing process.

### Characterization

Powder X-ray diffraction (XRD) patterns were measured on a Bruker D4 X-ray diffractometer (Germany) with Cu K$\alpha_1$ radiation ($\lambda$ = 1.5405 Å, 40 kV, 30 mA). Scanning electron microscopy (SEM) images were obtained from a Hitachi S-4800 microscope. Fourier transform infrared (FTIR) spectra were performed on a Bruker Vertex 70 FTIR spectrophotometer within the 4000–400 $cm^{-1}$ region using the KBr pellet method. The excitation and emission spectra were obtained on a Hitachi F-7000 fluorescence spectrophotometer with a 450 W xenon lamp as the excitation source. The UV-vis absorption spectra were recorded with a Shimadzu-UV-3101 scanning spectrophotometer. Excited-state decay curves with a microsecond grade were measured with a Lecroy Wave Runner 6100 Digital Oscilloscope (1 GHz) using a tunable laser as the excitation source (Continuum Sunlite OPO), and nanosecond grade decay curves were measured with a FL980 fluorescence lifetime spectrometer (Edinburgh) using a hydrogen flash lamp as the excitation source. Lifetimes were calculated by exponential fitting. The photoluminescence quantum yield (PLQY) values were measured directly with an absolute PLQY measurement system using FL980 with its corresponding integrating sphere and corresponding software.

### Preparation of Eu(BTC)

The nanoscale Eu(BTC) was prepared through an improved method as in a previous report.[24] In a typical synthesis, $Eu(NO_3)_3{\cdot}6H_2O$ (178 mg, 0.4 mmol) was dissolved in 20 mL of double distilled water and then NaAc (164 mg, 1.2 mmol) was added to form a metal precursor solution. $H_3BTC$ (88 mg, 0.4 mmol) was dissolved in 20 mL of ethanol with ultrasonic agitation to form an organic ligand solution. These two solutions were mixed with magnetic stirring at room temperature and a large amount of white suspension was generated immediately. After vigorous stirring for an hour, the product was collected by centrifugation, washed three times with ethanol and water and dried overnight at 60 °C.

### Synthesis of rhodamine 6G hydrazide (RGH)

In this work, RGH was synthesized according to a similar procedure as previously described.[25] Rhodamine 6G (1.20 g, 2.5 mmol) was dissolved in 30 mL of absolute ethanol. 3.0 mL (excess) of hydrazine hydrate (85%) was then added dropwise to the solution with vigorous stirring at room temperature. After the addition, the stirred mixture was refluxed in an oil bath for 10 h. The color of the solution changed from dark red to light orange and a colorless precipitate appeared. Then the precipitate was filtered and washed with 30 mL of water three times. The pale colored powder was dried under vacuum at 60 °C and the yield was 84%.

### Post-synthesis of RGH–Eu(BTC)

Eu(BTC) (93.4 mg 0.2 mmol), EDC (76.7 mg 0.4 mmol), and NHS (46 mg 0.4 mmol) were dispersed in 20 mL of anhydrous ethanol and stirred for 15 min at room temperature. Then equivalent RGH (85.6 mg, 0.2 mmol) with 4 mL of DMF was added into the above solution and stirred for 24 h sufficiently at room temperature. The white powder was collected and thoroughly washed with water and DMF several times to remove the residual EDC, NHS and unconnected rhodamine probe on the surface of the MOF.

### Detection of picric acid

In a typical detection process of PA, 2.5 mg of RGH–Eu(BTC) was dispersed in 50 mL of ethanol to make the suspension concentration 0.05 mg $mL^{-1}$. Each time, a 2.0 mL suspension of RGH–Eu(BTC) was added to a 1 cm quartz cuvette and excited at 285 nm. Then various concentrations of PA were injected into the suspension, and the corresponding fluorescence spectra were recorded. The selectivity investigation with other nitroaromatic compounds and organic carboxylic acids were performed under identical conditions. In addition, the spectra were recorded more than 3 times, and the average values were used to determine the intensity ratio $I_{555}/I_{616}$.

# Results and discussion

### Structural properties of RGH–Eu(BTC) chemosensors

The synthetic protocol of RGH–Eu(BTC) and its principle for PA detection are graphically represented in Scheme 1. XRD patterns of Eu(BTC), RGH–Eu(BTC) and RGH–Eu(BTC) treated with PA ethanol solution for a month are shown in Fig. 1. The pattern for as-synthesized Eu(BTC) is similar to that for La(BTC)·$6H_2O$

 

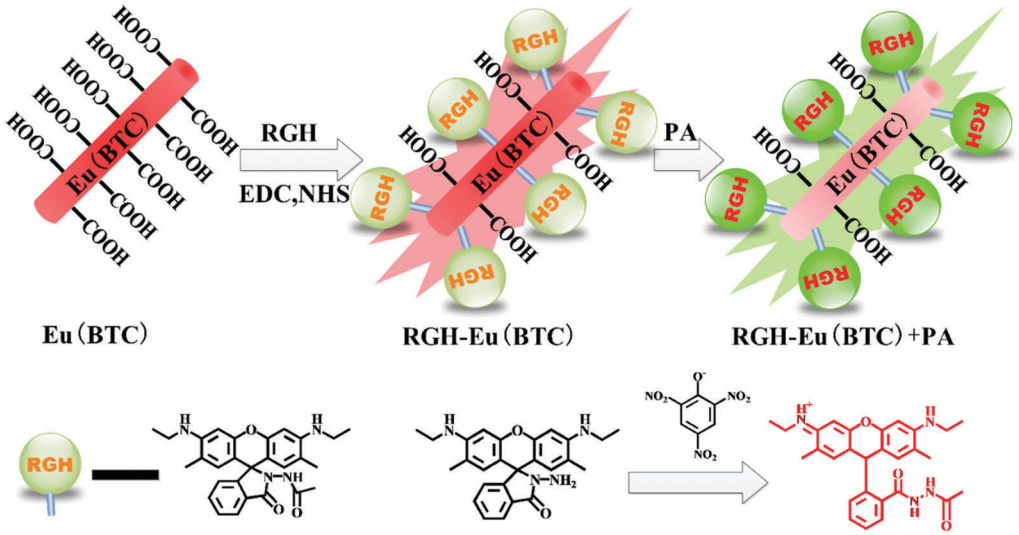


Scheme 1 The synthetic protocol of RGH–Eu(BTC) and its principle for PA detection.

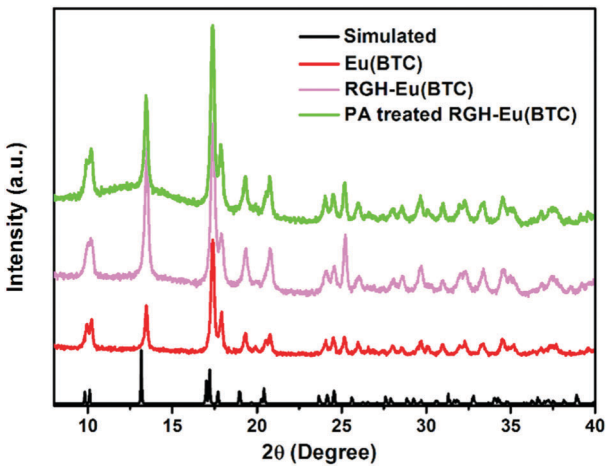


Fig. 1 X-ray powder diffraction patterns of La(BTC)·6$H_2O$ simulated (black); Eu(BTC) (red); RGH–Eu(BTC) (pink); and PA treated RGH–Eu(BTC) (green).

(CCDC: 290771) reported in previous literature.[26] Compared with Eu(BTC), RGH–Eu(BTC) and PA solution treated RGH–Eu(BTC) exhibit identical diffraction peaks in the 2$\theta$ range from 8° to 40°, suggesting that their crystalline structures are retained. This means that the framework is stable during the preparation process and the detection experiment. The SEM images are shown in Fig. S1 (ESI†). The Eu(BTC) has a smooth surface and a rod-like shape but not a uniform size ranging from 60 nm to 100 nm in width and 200 nm to 2 μm in length. As the size of the rhodamine probe (RGH) was only a few nanometers, the shape and size of RGH–Eu(BTC) were not changed clearly after modifying the rhodamine probe (RGH) onto the surface of the luminescent lanthanide MOF (Eu(BTC)). But the organic molecular probe made the surface of RGH–Eu(BTC) become much rougher than that of unmodified Eu(BTC).

The FTIR spectra of Eu(BTC), RGH, RGH–Eu(BTC) and mixed RGH and Eu(BTC) (denoted as RGH&Eu(BTC)) are shown in Fig. S2 (ESI†). Eu(BTC) displays characteristic absorption bands at 1615–1375 $cm^{-1}$ and 1110 $cm^{-1}$, which are assigned to the vibrations of carboxyl groups. The uncoordinated carboxylate groups were exposed on the surface of Eu(BTC) which provided reaction sites to graft with the rhodamine probe. A series of absorption bands at 2973 $cm^{-1}$ and 2929 $cm^{-1}$ are attributed to methylene group vibration (–$CH_2$–) absorption in the rhodamine moiety, which has been found in RGH and RGH–Eu(BTC) but not in Eu(BTC). Compared with Eu(BTC), new bands at 1688 $cm^{-1}$ and 1268 $cm^{-1}$ are observed in RGH–Eu(BTC), which are assigned to the vibration of C=O and C–N from RGH. To assess whether RGH and Eu(BTC) are one sample or a mixture, we also measured the FTIR spectra of a mixture sample. The result indicated that an amido bond (–$NH_2$) was retained. Thus, for RGH–Eu(BTC), the disappearance of the double absorption peaks at 3426 $cm^{-1}$ and 3344 $cm^{-1}$ for the amido bond (–$NH_2$) may suggest that RGH has been successfully grafted onto the surface of Eu(BTC). On the other hand, if RGH and Eu(BTC) are a mixture, RGH can be washed with DMF and separated from Eu(BTC) by centrifugation.

C, H, and N elemental analysis was also carried out to determine the content of the rhodamine derivative in the composite. The elemental analysis results of Eu(BTC) and RGH–Eu(BTC) are summarized in Table S1 (ESI†). In Eu(BTC), the content of C is 23.44 wt% from the $BTC^{3-}$ ligand, which is close to the theoretical value of 23.13 wt% in Eu(BTC)·6$H_2O$, and the trace amounts of N may be from the nitrate of the initial material. Compared with Eu(BTC), the increased percentages of C and N in RGH–Eu(BTC) are approximately 7.97 wt% and 1.48 wt%, respectively. Moreover, the increased C/N ratio in RGH–Eu(BTC) is 5.385, which is close to the theoretical C/N ratio 5.575 of RGH. Therefore, the content of the loaded rhodamine probe is only 10.94 wt%.

To evaluate the thermal stability of the sensor, the TG analysis of RGH–Eu(BTC) was carried out as shown in Fig. S3 (ESI†). The TG curve has two main weight losses. The first weight loss of 17% in the range of 50 °C and 150 °C is attributed to the loss of the solvent molecules and coordinated $H_2O$

molecules; and the second weight loss of 44% between 350 °C and 500 °C corresponds to the organic ligand and the rhodamine derivative. This result means that our sensor has good thermal stability.

### Fluorescence properties

The fluorescence properties of Eu(BTC), RGH, and RGH–Eu(BTC) have been investigated and their excitation and emission spectra at room temperature are displayed in Fig. S4 (ESI†) and Fig. 2. Eu(BTC) exhibits an excitation band from 200 to 320 nm with the maximum value at 268 nm. When PA is added, RGH has two peaks in the ultraviolet wavelength region which are attributed to the spirolactam ring structure, and another strong peak centered at 515 nm is attributed to the spirolactam ring-opening structure. Moreover, after covalent grafting with RGH, the excitation spectrum of Eu(BTC) has a 17 nm red-shift from 268 nm to 285 nm (Fig. S4c, ESI†), which may be caused by the decrease of energy for the large conjugated system. Although 515 nm is the maximum excitation of rhodamine, it could not arouse Eu emission. So 285 nm was chosen to excite both the rhodamine moiety and Eu(BTC) moiety. When excited at 285 nm, the RGH–Eu(BTC) gives a weak emission band at 543 nm and three narrow bands at 594, 616, and 692 nm, which are attributed to RGH emission (543 nm) and characteristic transitions ($^5D_0 \rightarrow {}^7F_J$, $J$ = 1, 2, 4) of Eu(BTC) (594, 616, and 692 nm). The missing emission of Eu at 650 nm may be due to the cross-relaxation process. The temporal stability result is displayed in Fig. S5 (ESI†). The fluorescence spectrum after being exposed in the air for a month was similar to the previous one, and the integrated intensities of $I_{550}/I_{616}$ were 0.167 (361, 2162.5) and 0.170 (374, 2197), respectively. This result indicated that the optical properties of the sensor were temporally stable.

### Fluorescence detection of PA

As previously reported, lanthanide MOFs exhibit marked luminescence quenching with electron deficient nitroaromatic compounds.[27] However, signals that depend on only one emission intensity usually require an additional calibration, thus a dual response for PA is significant. Considering that PA possesses two characteristic groups: an electron deficient nitro phenyl ring and an acidic hydroxyl group, we design the RGH–Eu(BTC) system as a ratiometric fluorescent sensor to recognize PA. In titration experiments, an ethanol solution of PA was added incrementally and the emission spectra were recorded. To make comparisons, the emission spectra of Eu(BTC), RGH and RGH–Eu(BTC) with different concentrations of PA were recorded as shown in Fig. 3a–c. The integrated intensities of their characteristic transitions are shown in Fig. S6 and S7 (ESI†) and Fig. 3d. As we can see, all three materials exhibit an obvious spectral change along with the addition of PA. For single materials, the fluorescence intensities exhibit a single change along with the addition of PA. RGH–Eu(BTC) exhibits an integrated PA concentration-dependent luminescence variation compared with single RGH and Eu(BTC). The green emission band at about 550 nm is increased, indicating the configuration transformation of RGH. It is noteworthy that the broad emission peak has a 12 nm red-shift from 543 nm to 555 nm which may be caused by forming a larger conjugated system between the RGH moiety and PA.

Although both RGH and Eu(BTC) could recognize PA, the sensitivity of RGH–Eu(BTC) has been improved when we immobilize the probe onto the surface of the MOF. Furthermore, such a sensitive PA sensor does not require any additional calibration of fluorescence intensity. The relationship between PA concentration and $I_{555}/I_{616}$ (the ratio of fluorescence intensity at 555 nm to that at 616 nm) is shown in Fig. 3d. The intensity ratio $I_{555}/I_{616}$ is 0.209 for the blank measurement (relative standard deviation, RSD = 4.76%), 0.371 for 2 μM (RSD = 5.47%), 0.437 for 5 μM (RSD = 5.37%), 0.535 for 10 μM (RSD = 3.67%), 0.723 for 20 μM (RSD = 1.83%), 0.982 for 30 μM (RSD = 3.03%), 1.280 for 40 μM (RSD = 1.71%), 1.467 for 50 μM (RSD = 4.18%), 1.682 for 60 μM (RSD = 6.55%), 2.077 for 80 μM (RSD = 8.49%), 2.463 for 100 μM (RSD = 7.5%), 4.196 for 200 μM (RSD = 3.6%), 6.081 for 450 μM (RSD = 1.84%) and 6.525 for 600 μM (RSD = 2.93%). These plots appear to show a linear increase at a low concentration range (2–200 μM) and bend upwards at a higher concentration (200–600 μM). The nonlinear performance of the relation curve can be accounted for by the interactions between the dye probe and luminescence MOFs, and the emission intensity at 616 nm is influenced by the emission band centered at 555 nm at high concentration. The concentration-dependent property is constructed with a good correlation coefficient ($R^2$ = 0.9946), and its corresponding linear regression equation is shown in Fig. 3d. As defined by IUPAC, the limit of detection (LOD) of RGH–Eu(BTC) for PA is calculated to be 0.45 μM/103.0 ppb ($3\alpha/S$), which is a very low level concentration. Moreover, the fluorescence spectral change is usually accompanied by the emission light changing from pink to yellow-green after introducing PA (Fig. 3d inset), which can be obviously observed by the naked eye under a lab UV lamp.

Interestingly, when excited at 510 nm, the RGH–Eu(BTC) sensor also acts as a ''turn on'' fluorescence sensor as shown in Fig. S8 (ESI†). After adding 600 μM PA, the emission intensity at 555 nm in RGH–Eu(BTC) is increased much more (approximately twentyfold) than that of a single RGH probe (approximately tenfold),

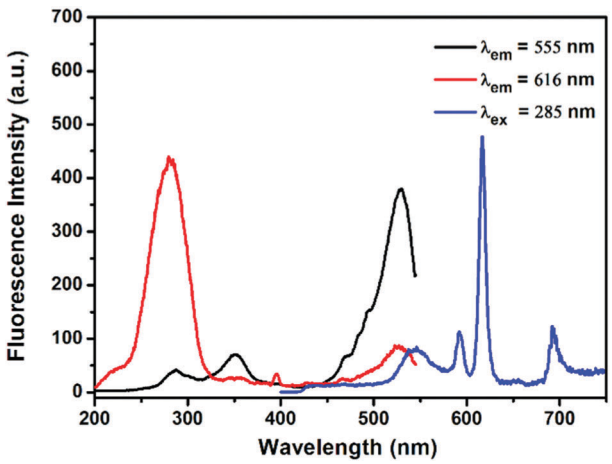


Fig. 2 The fluorescent excitation and emission spectra of RGH–Eu(BTC) + PA.

 

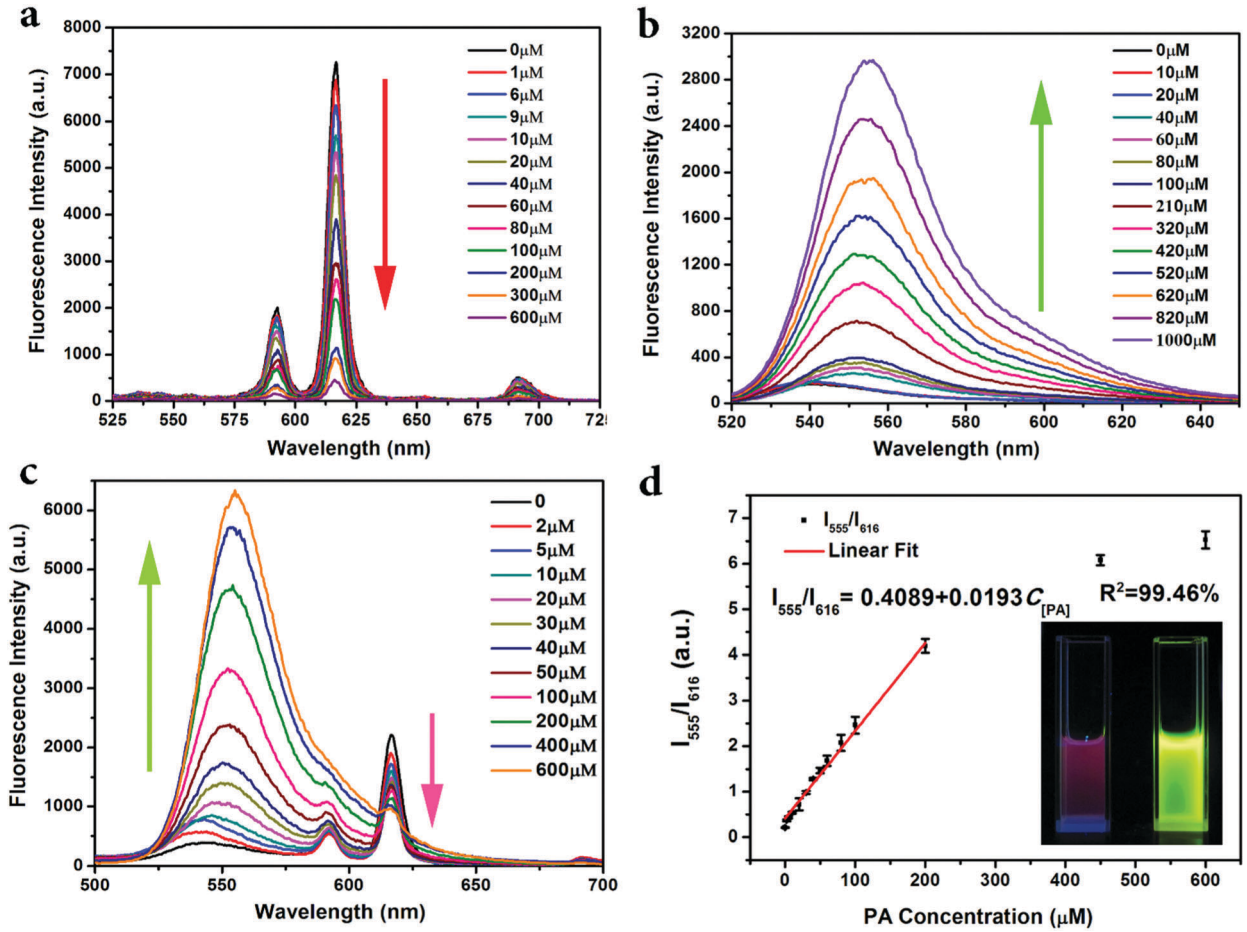


Fig. 3 Fluorescence spectra of (a) Eu(BTC) (0.05 mg $mL^{-1}$), (b) RGH (50 μM) and (c) RGH–Eu(BTC) (0.05 mg $mL^{-1}$) in the presence of various PA concentrations, and (d) plots of the relationship between the integrated intensity of $I_{555}/I_{616}$ and PA concentrations from 0 to 600 μM excited at 285 nm. Inset: Fluorescence images of RGH–Eu(BTC) and RGH–Eu(BTC) + PA under 254 nm UV light.

Table 1 Performance comparison of different nitro explosive detection methods

| Material | Analyte | LOD | Mechanism | Ref. |
|---|---|---|---|---|
| RGH–Eu(BTC) | PA | 0.45 μM | Ratio & off–on | This work |
| Tb-BTC | DNT | 0.1 mM/23 ppm | PL quenching | 20 |
| TABD–MOFs | NTO | 40 nM | PL turn on | 23 |
| MOF-3 | TNT | 0.9 ppb | PL quenching | 28 |
| Bio-MOF-1 | PA | 12.9 nM/2.9 ppb | PL quenching | 6 |
| $Eu_3(L)_3(HCOO)(\mu_3\text{-}OH)_2$ | PA | 4.98 μM | PL quenching | 29 |
| $[Cu(L)(I)]_{2n}$ | PA | 6.6 μM | PL quenching | 30 |
| $[Tb(1,3,5\text{-}BTC)]_n$ | PA | 81 nM | PL quenching | 27 |
| Zr(IV)–MOF | PA | 1.63 μM | PL quenching | 31 |
| Calix-SAM | Picrate | 0.3 ppm | UV-vis turn on | 32 |

which demonstrated that the rhodamine derivative probe in the dye-MOF system is more sensitive to PA than in the dye probe solution. What is more, incorporating the probe molecule into a solid matrix is beneficial to practical applications in PA sensing devices. To assess the potential application of RGH–Eu(BTC) as a ratiometric PA chemosensor, a comparison of the sensing performance of our method with some other previous works is listed in Table 1. Compared with other MOF materials for nitro explosives detection, the RGH–Eu(BTC) has a comparable detection limit and a more credible response mechanism. Moreover, Lupo *et al.* reported a functionalized complex, calix-SAM, which could recognize picrate by UV-vis spectra.[32] Thus, we also studied the UV-vis property of our hybrid material.

### Absorption properties of RGH–Eu(BTC) for PA

Since rhodamine derivatives exhibit a spirolactam ring opening structure in an acidic environment, the sensing properties of RGH and RGH–Eu(BTC) were further studied by UV-vis absorption spectroscopy. The absorbance spectra at various PA concentrations are shown in Fig. 4 and Fig. S9 (ESI†). Both RGH

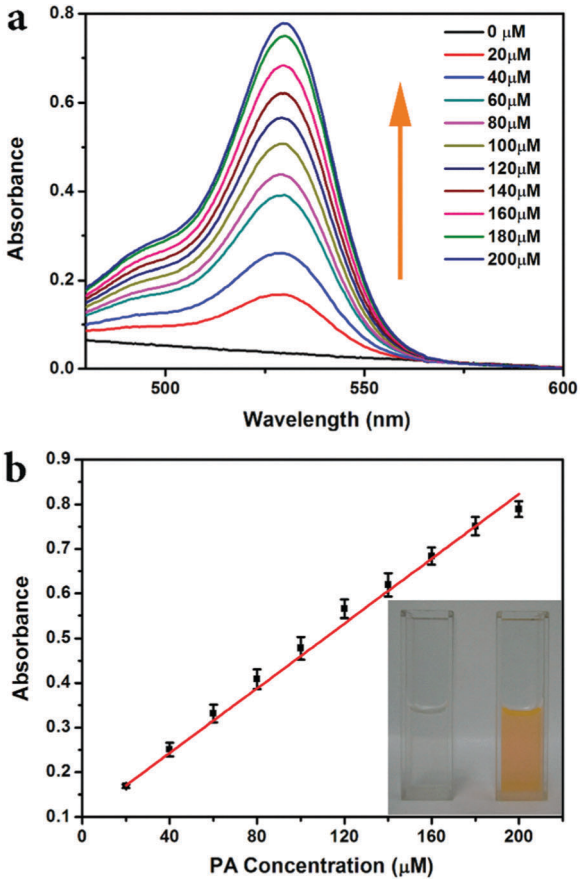


Fig. 4 (a) Absorption spectra of RGH–Eu(BTC) in the presence of various concentrations of PA. (b) The linear fitting plot of the absorption peak intensity at 529 nm. Inset: The visual color change between the original solution and after adding 100 μM PA.

and RGH–Eu(BTC) display a broad absorption band ranging from 475 nm to 550 nm with maximum values at 529 nm after adding PA. However, RGH–Eu(BTC) gives a more obvious color change than pure RGH, which may be attributed to the positive impact for ring opening from lanthanide MOFs. When the concentration of PA reached 20 μM, an obvious orange color can be observed with the naked eye. In the range of 20–200 μM, a good linearity was obtained with a coefficient of determination $R^2$ of 0.99, which provided dual mode detection of PA. The absorbance values of RGH–Eu(BTC) at 529 nm are 0.1685 for the blank measurement (relative standard deviation, RSD = 4.76%), 0.1685 for 20 μM (RSD = 2.15%), 0.251 for 40 μM (RSD = 6.15%), 0.331 for 60 μM (RSD = 5.78%), 0.409 for 80 μM (RSD = 5.39%), 0.478 for 100 μM (RSD = 5.27%), 0.566 for 120 μM (RSD = 3.7%), 0.619 for 140 μM (RSD = 4.21%), 0.6835 for 160 μM (RSD = 2.84%), 0.751 for 180 μM (RSD = 2.75%), 0.789 for 200 μM (RSD = 2.27%), 4.196 for 200 μM (RSD = 3.6%), 6.081 for 450 μM (RSD = 1.84%) and 6.525 for 600 μM (RSD = 2.93%). At the same time, a colorimetric change from colourless to orange is also observed as shown in the Fig. 4b inset. This result means that RGH–Eu(BTC) can detect PA not only as a fluorescent ratiometric sensor, but also as a good colorimetric sensor.

### Response time course

Response time is a significant indicator for PA explosive sensors, since the possibility of explosion may increase as time goes on. Fluorescence kinetics of RGH–Eu(BTC) in the presence of PA in ethanol was taken by monitoring the emission at 555 nm under 285 nm excitation at room temperature. As shown in Fig. 5, the initial fluorescence intensity of RGH in RGH–Eu(BTC) is very weak but stable. After mixing PA repeatedly (20 μM each time), this intensity increases rapidly and becomes steady in less than 25 s, and then remains nearly constant until the next addition. Thus RGH–Eu(BTC) can be a good sensor for real-time monitoring of PA.

### Selectivity and anti-interference performance

Special selectivity and anti-interference performance are important parameters for a sensor since the detection environment is usually complex. Hence, we investigated the response of RGH–Eu(BTC) toward other potentially interfering nitroaromatic compounds including *p*-nitrotoluene (NT), 4-nitrochlorobenzene (Cl-NB), 2,4-dinitrotoluene (DNT), trinitrotoluene (TNT), and 3-nitrophenol (3-NP), as well as other organic carboxylic acids including acetic acid (Ac), oxalic acid (Ox), malonic acid (Ma), phenol, and benzoic acid (BA) which may facilitate the spirolactam ring-opening process. All samples were tested under identical conditions and their fluorescent responses are illustrated in Fig. 6. The average values and RSD data of $I_{555}/I_{616}$ upon addition of different analytes are displayed in Table S2 (ESI†). It is worth noting that when the reference electrophilic nitroaromatic compounds were added to RGH–Eu(BTC), the emissions at both 555 nm and 616 nm were quenched, but the integrated ratio of $I_{555}/I_{616}$ was slightly or negligibly changed (Fig. S10, ESI†). Rhodamine derivatives usually display strong fluorescence under acidic conditions due to their structural change from spirocyclic to ring-opened forms, so the rhodamine moiety could not undergo spirolactam ring opening under acidic conditions. But thanks to the Eu–MOF moiety not being influenced by pH, we can detect picric acid by integrated variation. When organic carboxylic acids were added to the system, the

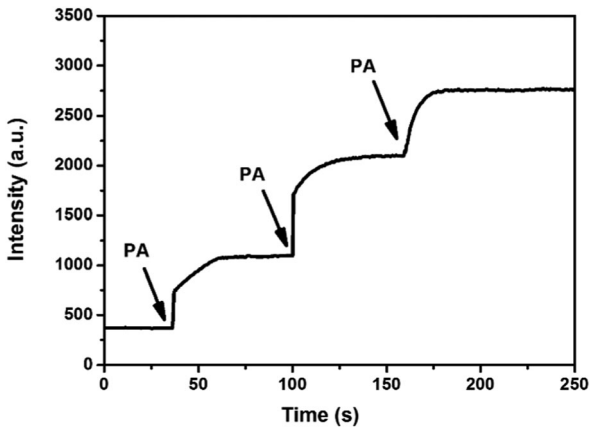


Fig. 5 Response time at 555 nm of RGH–Eu(BTC) with repeated addition of PA (20 μM) at room temperature, excited at 285 nm.

 

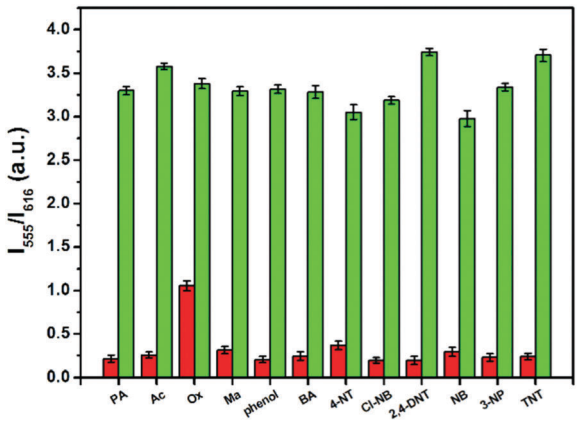


Fig. 6 The relative fluorescence intensity ($I_{555}/I_{616}$) changes upon addition of different analytes (red bars: the addition of various analytes individually; green bars: the coexistence of PA and the above analytes), excited at 285 nm.

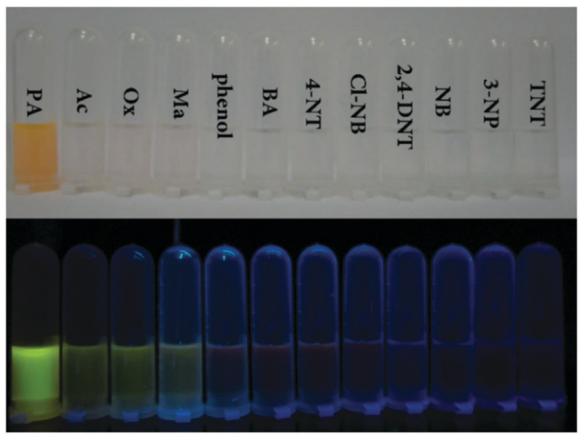


Fig. 7 Photographs of the colorimetric performance of RGH–Eu(BTC) (0.05 mg $mL^{-1}$) upon addition of different analytes in ethanol (upper: visible color; lower: fluorescent color).

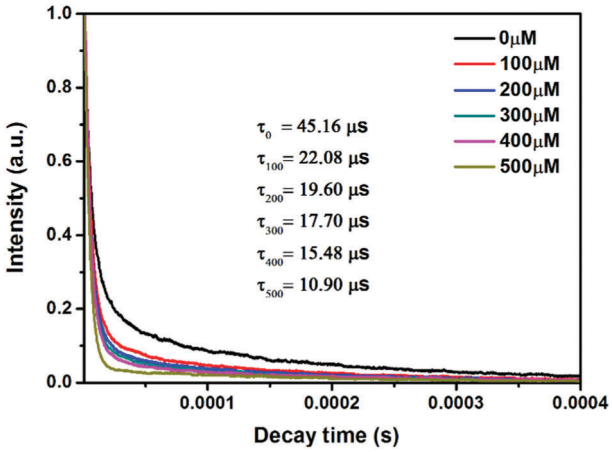


Fig. 8 Fluorescence decay curve of RGH–Eu(BTC) upon addition of PA at 616 nm.

emission at about 550 nm increased while the 616 nm emission remained unchanged. Thus, the effect of pH can also be distinguished from the change in the fluorescence spectra. Correspondingly, the colorimetric performance of RGH–Eu(BTC) (0.05 mg $mL^{-1}$) upon addition of different analytes in ethanol is shown in Fig. 7, which endowed this system with "naked eye" character in the detection of PA. After introducing PA, a remarkable fluorescence change can be observed, which indicates that RGH–Eu(BTC) has good selectivity and anti-interference performance for the detection of PA.

### Mechanism of ratiometric fluorescence specific for PA

In order to understand the origin of the RGH–Eu(BTC) sensing performance toward PA, the possible mechanism was investigated. As shown in Fig. S11 (ESI†) and Fig. 8, the lifetime of $Eu^{3+}$ in Eu(BTC) is 44% reduced in the absence and presence of PA. While in the RGH–Eu(BTC) sample, the excited state lifetime of $Eu^{3+}$ is obviously reduced (76%), which may be due to the fact that the RGH probe promotes the electron transfer process between the MOF and PA.[33,34] According to previous reports, the fluorescence quenching effect of lanthanide MOFs can be explained by a donor–acceptor electron transfer mechanism.[35,36] That is to say, the nitroaromatics are usually good electron acceptors due to the fact that the aromatic ring is replaced by the electron-withdrawing nitro groups with a lower energy of the empty π* orbitals, and the Eu(BTC) moiety in RGH–Eu(BTC) acts as an excellent electron-rich donor. Here, the high selectivity toward other nitro explosives may be attributed to the lower LUMO level of PA, and the excited electrons in the Eu(BTC) moiety could be more easily transferred to PA. Table S3 and Fig. S12 (ESI†) display the HOMO and LUMO energy levels of several nitroaromatics in this work as calculated at the B3LYP/6-31G* level of theory. In addition, supramolecular interactions (*e.g.* hydrogen bonding) between Eu(BTC) and PA may also facilitate the electron transfer between them.[37]

To more clearly illuminate the mechanism of RGH moiety changes after PA addition, we compared the absorption spectra of RGH, RGH–Eu(BTC), RGH + PA and PA as shown in Fig. S13 (ESI†). Both RGH and RGH–Eu(BTC) had absorption at 285 nm, but no significant absorption at 520 nm. When PA was added, the absorption at 520 nm appeared, and the one at 285 nm still remained. According to Beer's law, the molar absorption coefficient was calculated by $\varepsilon = A/CL$, where $C$ is the concentration of matter and $b$ is the optical length of the absorption cell. So the molar absorption coefficients in this work are $1.053 \times 10^3$ L $(mol\ cm)^{-1}$, $1.526 \times 10^4$ L $(mol\ cm)^{-1}$ and $7.880 \times 10^4$ L $(mol\ cm)^{-1}$ for PA, RGH and RGH–Eu(BTC), respectively. In the mixture of the two solutions (RGH + PA and RGH–Eu(BTC) + PA), the intensities of the RGH and RGH–Eu(BTC) emission are 6.45% and 1.32% reduced, respectively, which are influenced by the absorbance of picric acid at 285 nm. In addition, as PA is electron deficient, no emission of PA was observed at 285 nm excitation. So the increase in the fluorescence intensity and the shift in the fluorescence of RGH after PA addition may be caused by the opening of the spirolactam ring and the formation of the complex between PA and RGH.[16]

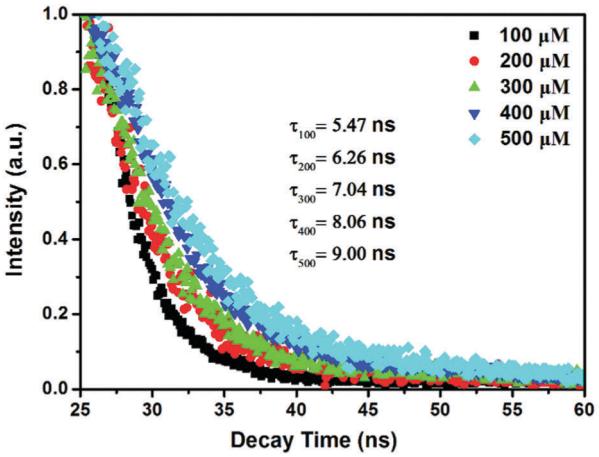


Fig. 9 Fluorescence decay curves of RGH–Eu(BTC) with different PA concentrations (100–500 μM) monitoring at 550 nm. Excited at 285 nm.

We also measured the PLQY values of RGH and RGH–Eu(BTC). In this work, we use rhodamine 6G as a standard sample, and its PLQY is 98.7%. The PLQY is calculated *via* the ratio of the number of photons emitted to the number of photons absorbed. In addition, the emission and scatter of the blank sample were measured and eliminated by background correction methods. The PLQY values of RGH in the absence and presence of PA are 5.8% and 62.3%, and those of RGH–Eu(BTC) are 16.7% and 93.2%, respectively. This result suggests that RGH–Eu(BTC) is more luminescent than RGH. In addition, the decay curves of RGH and RGH–Eu(BTC) with different PA concentrations were measured as shown in Fig. S14 (ESI†) and Fig. 9. The lifetime increased gradually with the addition of PA. This may be due to the ring-opening structure, which enhances the rigidity of the rhodamine derivative and reduces the non-radiative transition. Upon addition of organic carboxylic acids, limited fluorescence enhancement is observed at about 549 nm whereas the fluorescence at 616 nm does not show any variation (Fig. S10, ESI†). After adding PA, an opposite fluorescence change with an enhancement at 556 nm and a decrease at 616 nm is observed. Besides, oxalic acid, which has a similar p$K_a$ to PA (Table S4, ESI†), leads to an increased emission at 550 nm but unchanged emission at 616 nm. Therefore, the ratiometric RGH–Eu(BTC) sensor can detect PA by using an electron-rich luminescent MOF (Eu(BTC)) as an electron donor and an excellent fluorescent probe (RGH) as a recognition unit *via* configuration transformation from the spirolactam ring form to a ring-opened amide form. These dual response mechanisms cause RGH–Eu(BTC) to have a good PA detection performance.

### Practical applicability of RGH–Eu(BTC)

As the portability of a fluorescent sensor has already attracted extensive attention, we also study the practical applicability of RGH–Eu(BTC) for PA detection. Test strips were prepared by dipping filter paper strips into RGH–Eu(BTC) concentrated suspensions (5 mg $mL^{-1}$) and then drying in air. Then various concentrations of PA were added onto these test strips dropwise and a gradual colorimetric change from colourless to orange can be observed as shown in Fig. 10. This result demonstrates that the RGH–Eu(BTC) has outstanding sensing performance toward PA, which may provide a rapid and portable detection method to recognize PA with the naked eye.

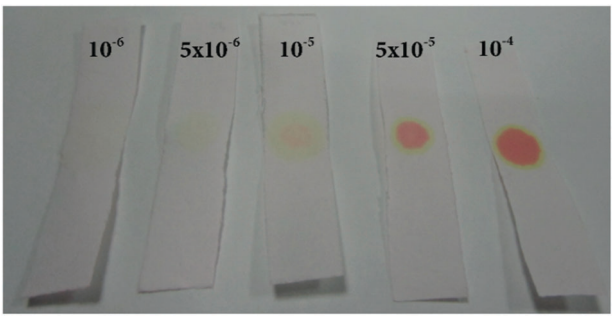


Fig. 10 Visible colour images of RGH–Eu(BTC) coated paper strips upon adding various concentrations of PA.

## Conclusion

In summary, this work presented a novel dual mode PA sensor by conjugating lanthanide MOFs with a rhodamine probe. RGH–Eu(BTC) could be used to precisely detect the PA concentration. Apart from the quantitative detection of PA *via* a spectroscopic method, the RGH–Eu(BTC) sensor also exhibited qualitative recognition of PA with the naked eye *via* a colorimetric method. Moreover, it displayed high sensitivity and selectivity toward PA over other nitroaromatic compounds and acidic analytes. The possible detection mechanism is discussed in this paper. As a real-time sensor, practical application with a test strip was also demonstrated. The dual mode sensing properties indicated that connecting a rhodamine moiety with luminescent MOFs might be a promising scenario to design a ratiometric PA sensor with remarkable detection properties.

## Acknowledgements

The authors gratefully thank the financial support from the NSFC (Grant No. 51372240, 51572256, 21501166, 21673218) and the Science and Technology Developing Project of Jilin Province (Grant No. 20170520135JH).

## Notes and references

1 S. S. Nagarkar, A. V. Desai and S. K. Ghosh, *CrystEngComm*, 2016, **18**, 2994–3007.
2 R. Chopra, V. Bhalla, M. Kumar and S. Kaur, *RSC Adv.*, 2015, **5**, 24336–24341.
3 V. Pimienta, R. Etchenique and T. Buhse, *J. Phys. Chem. A*, 2001, **105**, 10037–10044.
4 S. Shanmugaraju and P. S. Mukherjee, *Chem. Commun.*, 2015, **51**, 16014–16032.
5 G. Sivaraman, B. Vidya and D. Chellappa, *RSC Adv.*, 2014, **4**, 30828.

 

6 B. Joarder, A. V. Desai, P. Samanta, S. Mukherjee and S. K. Ghosh, *Chemistry*, 2015, **21**, 965–969.
7 Y. Xu, B. Li, W. Li, J. Zhao, S. Sun and Y. Pang, *Chem. Commun.*, 2013, **49**, 4764–4766.
8 M. E. Walsh, *Talanta*, 2001, **54**, 427–438.
9 J. M. Sylvia, J. A. Janni, J. D. Klein and K. M. Spencer, *Anal. Chem.*, 2000, **72**, 5834–5840.
10 Y. Salinas, R. Martinez-Manez, M. D. Marcos, F. Sancenon, A. M. Costero, M. Parra and S. Gil, *Chem. Soc. Rev.*, 2012, **41**, 1261–1296.
11 M. E. Germain and M. J. Knapp, *Chem. Soc. Rev.*, 2009, **38**, 2543–2555.
12 P. Lutsyk, R. Arif, J. Hruby, A. Bukivskyi, O. Vinijchuk, M. Shandura, V. Yakubovskyi, Y. Kovtun, G. A. Rance, M. Fay, Y. Piryatinski, O. Kachkovsky, A. Verbitsky and A. Rozhin, *Light: Sci. Appl.*, 2016, **5**, e16028.
13 J. Ma, T. Lin, X. Pan and W. Wang, *Chem. Mater.*, 2014, **26**, 4221–4229.
14 S. S. Nagarkar, B. Joarder, A. K. Chaudhari, S. Mukherjee and S. K. Ghosh, *Angew. Chem., Int. Ed.*, 2013, **52**, 2881–2885.
15 P. Wang, Y. Wang and L. Tong, *Light: Sci. Appl.*, 2013, **2**, e102.
16 V. Nagarajan and B. Bag, *Org. Biomol. Chem.*, 2014, **12**, 9510–9513.
17 P. Zhou, D. Zhou, L. Tao, Y. Zhu, W. Xu, S. Xu, S. Cui, L. Xu and H. Song, *Light: Sci. Appl.*, 2014, **3**, e209.
18 W. Zhang, G. Lu, S. Li, Y. Liu, H. Xu, C. Cui, W. Yan, Y. Yang and F. Huo, *Chem. Commun.*, 2014, **50**, 4296–4298.
19 S. N. Zhao, X. Z. Song, M. Zhu, X. Meng, L. L. Wu, J. Feng, S. Y. Song and H. J. Zhang, *Chemistry*, 2015, **21**, 9748–9752.
20 N. Campagnol, E. R. Souza, D. E. De Vos, K. Binnemans and J. Fransaer, *Chem. Commun.*, 2014, **50**, 12545–12547.
21 M. J. Dong, M. Zhao, S. Ou, C. Zou and C. D. Wu, *Angew. Chem., Int. Ed.*, 2014, **53**, 1575–1579.
22 Y. Cui, R. Song, J. Yu, M. Liu, Z. Wang, C. Wu, Y. Yang, Z. Wang, B. Chen and G. Qian, *Adv. Mater.*, 2015, **27**, 1420–1425.
23 Y. Guo, X. Feng, T. Han, S. Wang, Z. Lin, Y. Dong and B. Wang, *J. Am. Chem. Soc.*, 2014, **136**, 15485–15488.
24 K. Liu, H. You, Y. Zheng, G. Jia, L. Zhang, Y. Huang, M. Yang, Y. Song and H. Zhang, *CrystEngComm*, 2009, **11**, 2622.
25 L. Wang, B. Li, L. Zhang, L. Zhang and H. Zhao, *Sens. Actuators, B*, 2012, **171–172**, 946–953.
26 Y. Wen, J. Cheng, Y. Feng, J. Zhang, Z. Li and Y. Yao, *Chin. J. Struct. Chem.*, 2005, **24**, 1440.
27 J.-D. Xiao, L.-G. Qiu, F. Ke, Y.-P. Yuan, G.-S. Xu, Y.-M. Wang and X. Jiang, *J. Mater. Chem. A*, 2013, **1**, 8745.
28 B. Gole, A. K. Bar and P. S. Mukherjee, *Chemistry*, 2014, **20**, 2276–2291.
29 X.-Z. Song, S.-Y. Song, S.-N. Zhao, Z.-M. Hao, M. Zhu, X. Meng, L.-L. Wu and H.-J. Zhang, *Adv. Funct. Mater.*, 2014, **24**, 4034–4041.
30 S. Khatua, S. Goswami, S. Biswas, K. Tomar, H. S. Jena and S. Konar, *Chem. Mater.*, 2015, **27**, 5349–5360.
31 M. Sk and S. Biswas, *CrystEngComm*, 2016, **18**, 3104–3113.
32 F. Lupo, C. Capici, G. Gattuso, A. Notti, M. F. Parisi, A. Pappalardo, S. Pappalardo and A. Gulino, *Chem. Mater.*, 2010, **22**, 2829–2834.
33 L. H. Cao, F. Shi, W. M. Zhang, S. Q. Zang and T. C. W. Mak, *Chem. – Eur. J.*, 2015, **21**, 15705–15712.
34 W. Xie, S. R. Zhang, D. Y. Du, J. S. Qin, S. J. Bao, J. Li, Z. M. Su, W. W. He, Q. Fu and Y. Q. Lan, *Inorg. Chem.*, 2015, **54**, 3290–3296.
35 X. L. Hu, C. Qin, X. L. Wang, K. Z. Shao and Z. M. Su, *Chem. Commun.*, 2015, **51**, 17521–17524.
36 H. Ma, B. Li, L. Zhang, D. Han and G. Zhu, *J. Mater. Chem. A*, 2015, **3**, 19346–19352.
37 M. Liu, G. Li and Z. Cheng, *New J. Chem.*, 2015, **39**, 8484–8491.